103758
2

Development of Novel Electrolyte Materials for a New Generation of Low-Temperature SOFCs

Final Report for Year 2

Reporting Period: June 1, 2006 – February 28, 2007

Submitted to

Dr. Masaharu Hatano
Technology Research Laboratory No.1
Nissan Research Center
Nissan Motor Co., Ltd
1, Natsushima-Cho, Yokosuka-Shi
Kanagawa 237-8523, Japan
Phone: +81-46-867-5158; Fax: +81-46-865-8104
E-mail: m-hatano@mail.nissan.co.jp

Prepared by

C. Zuo, J. H. Wang, and M. Liu
Center for Innovative Fuel Cell and Battery Technologies
Georgia Institute of Technology
771 Ferst Drive
Atlanta, GA 30332-0245, USA
Tel: 404-894-6114; Fax: 404-894-9140
E-mail: meilin.liu@mse.gatech.edu

Principal Investigator: ___ ; **Date:** February 19, 2007

Meilin Liu

ABSRACT

While the advantages of low-temperature solid oxide fuel cells (SOFCs) are well known, suitable electrolytes for operation below 500 °C are still lacking. The discovery of a new solid electrolyte with high ionic conductivity is necessary in order to develop a new generation of SOFCs desirable for automobile applications. The objective of this project is to identify or create novel electrolyte materials suitable for this application. The research has been focusing mostly on improvement of oxide ion and proton conductivity of various electrolyte materials via increasing the mobile charge carrier density.

The materials based on A-site-K-doped and B-site-Y-doped $Ba(Zr,Ce)O_3$ have demonstrated both high ionic conductivity and adequate stability. In fact, the ionic conductivities below 500 °C exceed those of the best oxide ion conductors ever studied. We have systematically investigated these materials for low-temperature SOFCs. The chemical stability and proton conductivity were optimized by adjusting the compositions. A conductivity of 7×10^{-3} S/cm was achieved at 500 °C in humid 4% H_2/Ar atmosphere for B-site optimized material $Ba(Zr_{0.1}Ce_{0.7}Y_{0.2})O_3$ [BZCY7] which is much higher than that for YSZ (5×10^{-4} S/cm), and even better than that for GDC (5×10^{-3} S/cm). Furthermore, the A-site-K-doped $Ba(Zr,Ce)O_3$ demonstrate even better ionic conductivity at higher temperature. Initial results indicated that these electrolytes showed good chemical stability in the CO_2 atmosphere. There was no phase change after exposure to 2% CO_2 (bal. H_2) up to one week.

We fabricated single fuel cells based on the newly developed electrolytes by a modified dry pressing method, which allowed us to obtain a crack-free electrolyte membrane with 50 μm thickness. Fuel cell testing indicated that the cathode-electrolyte interfacial polarization resistance was the determining factor that limited the fuel cell performance. Thus, we further developed a new cathode materials - $Ba(Ce_{0.4}Pr_{0.4}Y_{0.2})O_3$. When Ni and BCPY4 were applied as anode and cathode materials, respectively, for the $Ba(Zr,Ce)O_3$-based fuel cells, maximum power densities reached 189, 157, 130, 94, and 61 mW cm^{-2} at 700, 650, 600, 550, and 500°C, respectively. These preliminary results indicate that BCPY4 appear to have the potential as the cathode materials for $Ba(Zr,Ce)O_3$ electrolyte based fuel cells.

Table of Contents

1. Introduction

For reasons related to long term stability and cost, reduction in operation temperature of solid oxide fuel cells (SOFCs) down to 650-800 °C has attracted interest world wide. Furthermore, if the operation temperature can be reduced to 400-500 °C, SOFC will be a promising candidate to replace internal combustion engines in vehicles, or be used as auxiliary power unit (APU) that operates independently from the main engine.

Successful reduction in operating temperature, however, requires new electrolytes with highly ionic conductivity and active electrodes to reduce interfacial polarization resistances. The solid oxide electrolyte is the heart of the SOFC; it must be free of porosity and should be thin to minimize ohmic loss. The electrolyte must have high ionic conductivity, but minimum (as close to zero as possible) electronic conductivity. In addition, the solid oxide electrolyte must be stable and exhibit pure ionic conductivity over a wide range of oxygen partial pressure (eg., 1 to 10^{-20} atm).

To date, many types of materials with oxygen-ion conductivity have been studied as solid electrolytes for SOFCs. Shown Figure 1.1.1 are the conductivities of several materials that have been widely studied, including stabilized zirconia-, doped ceria-, $LaGaO_3$-, and δ-Bi_2O_3/$Bi_4V_2O_{11}$-based electrolytes. Other electrolytes include:

1) materials based on $La_2Mo_2O_9$,

2) perovskite- and brownmilillеite-like phases derived from $Ba_2In_2O_5$,

3) perovskite-based on $LnBO_3$ (B=Al,In,Sc,Y),

4) solid electrolytes with apatite structure $A_{10-x}(MO_4)_6O_{2\pm\delta}$ (M=Si or Ge; A=Ln or alkaline earth cations), and

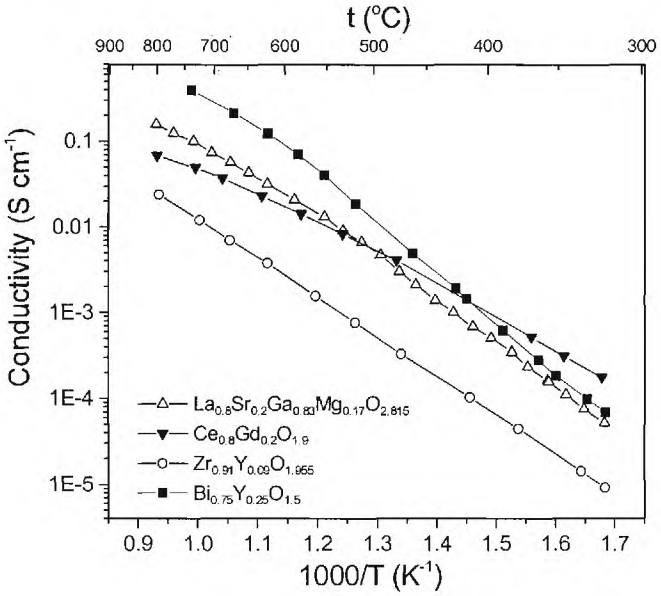

Figure 1.1.1. Comparison of the ionic conductivity as a function of temperature for various solid electrolytes in air.

5) Pyrochlores and fluorite-type $(Y,Nb,Zr)O_{2-\delta}$.

Among all of these solid electrolytes, only $Ce_{0.9}Gd_{0.1}O_{1.95}$ (GDC) can quite match the requirements to operate related SOFCs at temperatures below 500°C, due to its higher electrical conductivity and good interfacial properties when used as electrodes. However, doped ceria still has some critical issues to be addressed, including electronic conduction at the anode side and poor mechanical properties under fuel cell conditions.

So far, a suitable electrolyte for low-temperature SOFCs is still lacking. The discovery of a brand new solid electrolyte may result in a new generation of SOFCs.

The objective of this project is to identify or create novel solid electrolytes. The research has been focused on improving the ionic conductivity of the electrolyte material via increasing its mobile charge carrier density. Specifically, the materials is based on A-site-K-doped and B-site-Y-doped $BaZrO_3$.

2. Solid-State Proton Conductors

2.1. B-site-Y-Doped $Ba(Zr,Ce,Y)O_3$

2.1.1. Optimization of $Ba(Zr,Ce,Y)O_3$

The BZCY7 powder was prepared using a glycine nitrate combustion process. In this process, stoichiometric amounts of $Ba(NO_3)_2$, $Ce(NO_3)_3$, $Y(NO_3)_3$, and $ZrO(NO_3)_2$ were dissolved in water, a suitable HNO_3 (4N) was added to prevent the precipitation of $ZrO(NO_3)_2$. The solution was then mixed with glycine and heated on a hot plate to vaporize water, convert to gel, and finally ignite to flame, resulting in fine ash of pale yellow color. The resultant ash was then fired at 600 °C for 2 h to form the "foam" BZCY7 powder. In here, the NH_2CH_2COOH (glycine) can form complexes with metal ions, prevent selective precipitation, and make the metals mixed at atomic level; it is also the fuel for combustion during the reaction. Below are the reactions:

$$2Ba(NO_3)_2 + 2NH_2CH_2COOH \rightarrow BaO + 4CO_2 + 5H_2O + (2N_2 + NO + NO_2)$$

$$2Ce(NO_3)_3 + 2NH_2CH_2COOH \rightarrow 2CeO_2 + 4CO_2 + 5H_2O + (4N_2 + NO + NO_2)$$

$$2Y(NO_3)_3 + 2NH_2CH_2COOH \rightarrow 2Y_2O_3 + 4CO_2 + 5H_2O + (4N_2 + 2NO + NO_2)$$

$$2ZrO(NO_3)_2 + 2NH_2CH_2COOH \rightarrow 2ZrO_2 + 4CO_2 + 5H_2O + (2N_2 + NO + 2NO_2)$$

X-ray diffraction analysis (Figure 2.1) showed that the product had a same single phase as the powders made by solid state reaction.

Shown in Figure 2.2 (a) is SEM picture of a BZCY7 powder made by solid state reaction method, the size is about 2 μm and appear fully dense. In comparison, shown in Figure 2.2 (b) and (c) are SEM pictures of an as-synthesized BZCY7 particle made by GNP method, which is highly porous, and the pore size ranges from tens of nanometers to a micrometers. The powder is thus called a "foam" powder. It is this extremely low fill density that makes it possible to prepare thin films of BZCY7 by dry pressing.

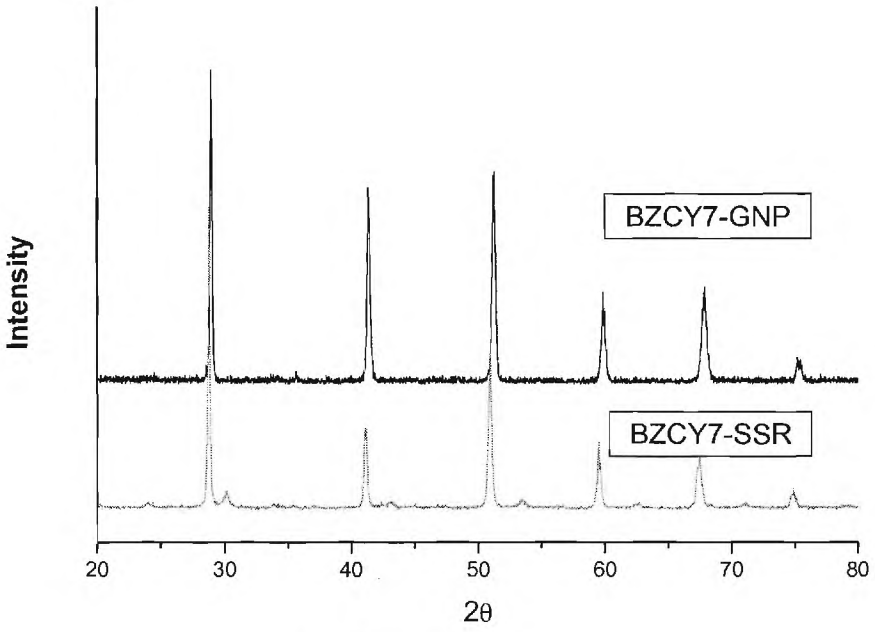

Figure 2.1 *X-ray diffraction patterns of the BZCY7 powder synthesized by glycine nitrate process and solid state reaction.*

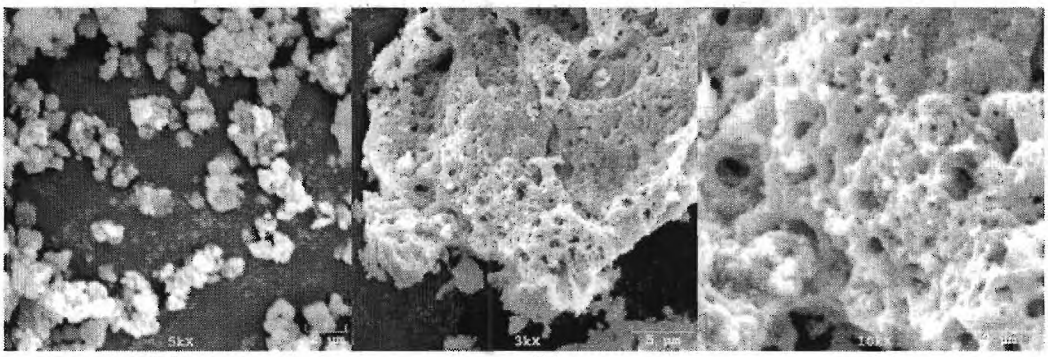

(a) (b) (c)

Figure 2.2 *SEM pictures of (a) BZCY7 made by SSR method (b) a highly porous "foam" BZCY7 particle, (c) a portion of the particle shown in (b).*

2.1.2. Chemical stability of $Ba(Zr,Ce,Y)O_3$

Chemical Stability in CO_2-Containing Atmospheres: The main concern on chemical stability is the possibility of reaction between perovskite-type materials with CO_2. For example, doped $BaCeO_3$ has been studied as an electrolyte material for SOFC. While its ionic conductivity is sufficiently high, the chemical stability in CO_2- or H_2O-containing atmospheres is inadequate for fuel cell applications.

The proposed reaction of ABO_3 with CO_2 is:

$$ABO_3 + CO_2 = ACO_3 + BO_2$$

where A represents Ba and B represents Ce in doped $BaCeO_3$ case.

To test the stability of BZCY7 material in CO_2-containing atmospheres, we monitored the conductivity as a function of time upon exposure to varying concentrations of CO_2/H_2 gas at 500 °C. Fig. 2.3 shows the time dependence of the conductivity of a BZCY7 symmetric cell samples (with Pt as electrode) tested using wet CO_2/H_2 gas that contained 10%, 20%, and 25% CO_2 (balance of H_2) at 500 °C.

Before and after each given concentration CO_2 stability measurement, the conductivity of BZCY7 symmetric cell samples (with Pt as electrode) was tested using wet H_2 gas for one day. After measurement of the conductivity in wet H_2, a given CO_2 concentration was introduced into furnace (10%, 20%, and 25% CO_2 /balance of H_2) for 4 or 5 days.

From Fig. 2.3, we can see that the conductivity was stable for 5 days in atmospheres containing up to 20% CO_2. Because the unexpected broken of our wire connection, the stability study was stopped after switched to 25% CO_2 containing atmosphere for 3 days. This preliminary result indicates that the BZCY7 is chemistry stable in 25% CO_2-containing atmospheres, and might be suitable for practical applications. And after the stability study in CO_2 containing gas, the conductivity was recovered back to the initial flux when switched the feed gas back to H_2.

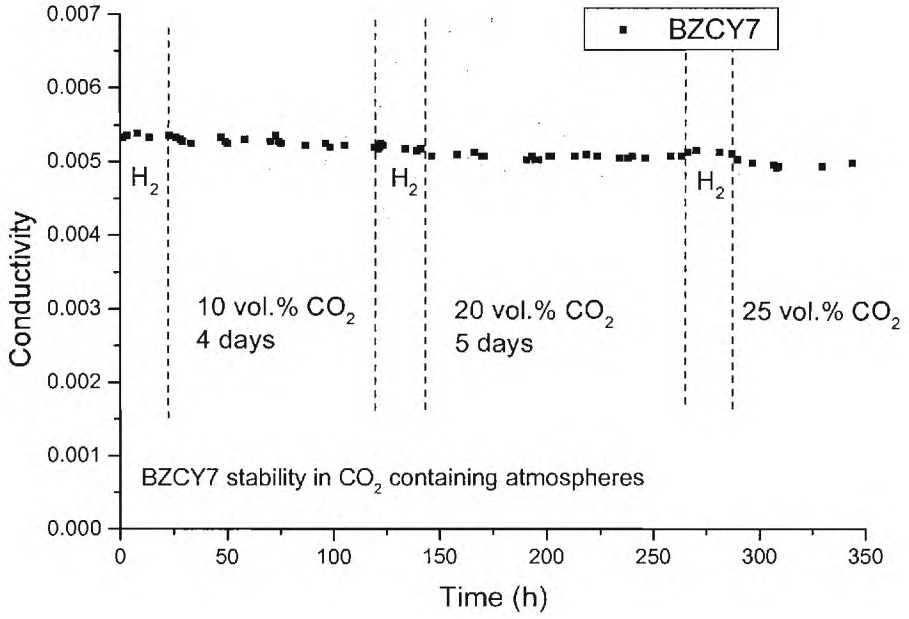

Figure 2.3 *Time dependence of conductivity for a BZCY7 symmetric cell in wet CO_2 (balance with H_2) atmospheres at 500 °C.*

The X-ray diffraction patters shown in Fig. 2.4 suggest that BCY20 were decomposed to $BaCO_3$, CeO_2, and Y_2O_3 after exposed to CO_2, whereas BZCY7 remained

the same, as compared with the XRD pattern before exposed to CO_2 atmosphere. These results indicate that BZCY7 is stable up to 25% CO_2 containing atmosphere at 500 °C.

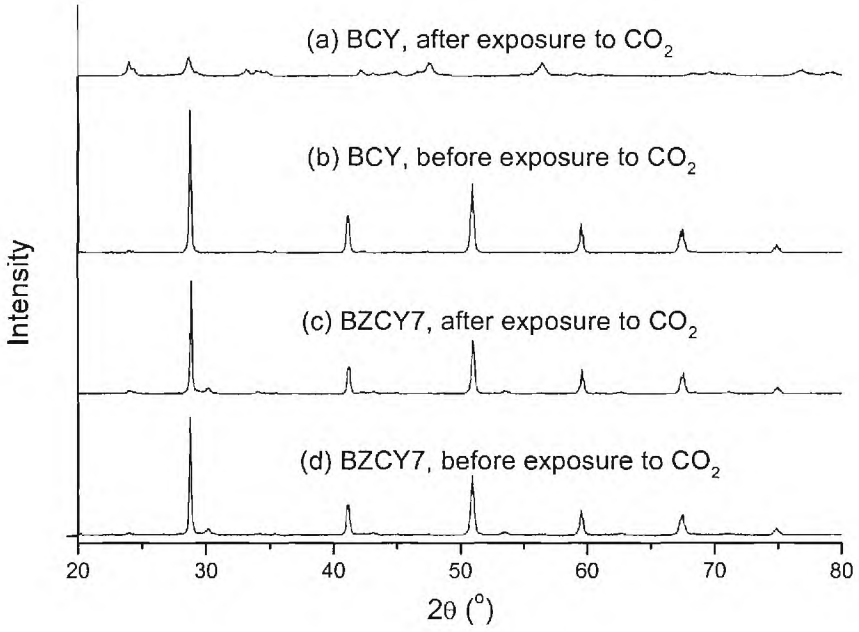

***Figure 2.4** X-ray diffraction patterns for BCY20 and BZCY7 before and after exposure to dry H_2 with 25 vol.% CO_2 at 500 °C.*

Chemical Stability in H_2O-Containing Atmospheres: In order to be the electrolyte materials for SOFCs, the material must be chemically and dimensionally stable in atmospheres containing H_2O among other constituents (the typical condition of fuel cell operation).

The proposed reaction of ABO_3 with H_2O is:

$$ABO_3 + H_2O = A(OH)_2 + BO_2$$

where A represents Ba and B represents Ce in doped $BaCeO_3$ case.

To test the stability of BZCY7 material in H_2O-containing atmospheres, we monitored the conductivity as a function of time upon exposure to varying concentrations of H_2O/H_2 gas at 500 °C. Fig. 2.5 shows the time dependence of the conductivity of a BZCY7 symmetric cell samples (with Pt as electrode) tested using wet 4% H_2/Ar gas that contained 20 and 50% H_2O at 500 °C.

Before and after water stability measurement, the conductivity of BZCY7 symmetric cell samples (with Pt as electrode) were tested using wet 4% H_2 gas (balance of Ar) for a week. After measurement of the conductivity in wet 4% H_2/Ar, a given H_2O concentration was introduced into furnace (20% and 50% water vapor content gas was obtained by bubbling H_2 gas through deionized water at 65 °C and 85 °C) for one week.

From Fig. 2.5, the conductivity was found to decrease moderately in the first several hours of exposure after switched to each given H_2O concentration gas mixer. The initial drops increased as the H_2O content increased from 20% to 50%, but after this

initial decrease, the hydrogen fluxes were stable for a week in atmospheres containing up to 50% H_2O. This preliminary result indicates that the BZCY7 is chemistry stable in up to 50% H_2O-containing atmospheres, and might be suitable for practical applications.

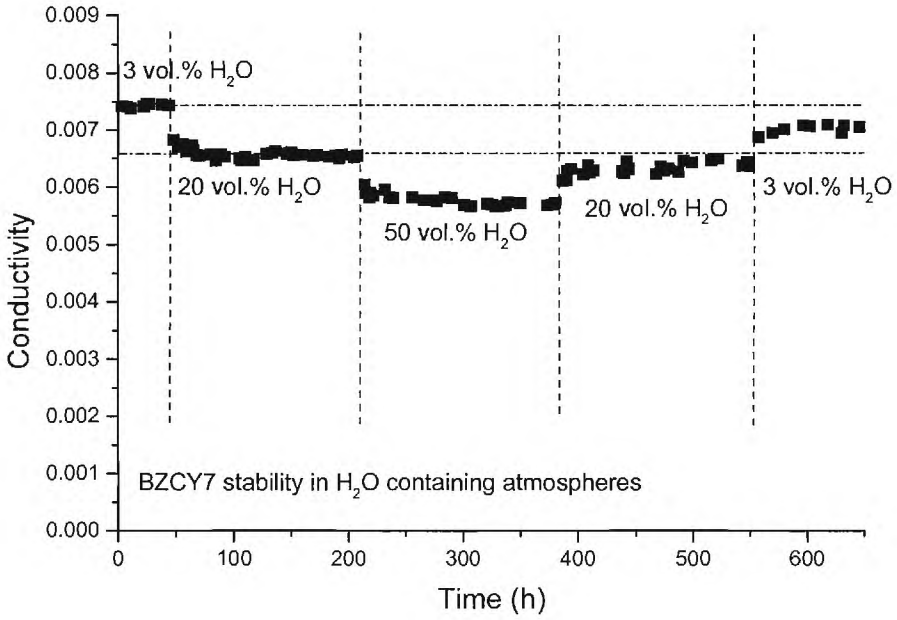

Figure 2.5 *Time dependence of conductivity for a BZCY7 symmetric cell in H_2O (balance with H_2/Ar) atmospheres at 500 °C.*

And after the stability study in H_2O containing gas, the conductivity was not fully recovered back to the initial point when switched back to 4% H_2/Ar, the possible reason is due to the Pt current collector's resistance increased as the time increased in higher water vapor containing atmospheres. As shown in Fig. 2.6, the electrode's resistance of the BZCY7 symmetric cell increased at each time when we increased the H_2O concentrations, and can not fully recover back after we decreased the H_2O concentration to the 3% when we finished the stability testing. This also can be observed by using the ohm meter to directly measure the resistance of the Pt electrode before and after the stability testing.

As indicated in Fig. 2.7, the XRD examination on BZCY7 powder sample after exposure to 50% H_2O/H_2 atmosphere showed that it remained the exactly same perovskite structure by comparing with the XRD pattern before exposed to H_2O-containing atmospheres. This preliminary experiment results indicate that the BZCY7 material is stable up to 50% water vapor containing atmosphere at 500 °C.

As indicated in Fig. 2.8, the Roman examination on BZCY7 disk sample after exposure to 50% H_2O/H_2 atmosphere showed that it remained the exactly same perovskite structure by comparing with the Roman pattern before exposed to H_2O-containing atmospheres. This experiment results also confirmed that the BZCY7 material is stable up to 50% water vapor containing atmosphere at 500 °C.

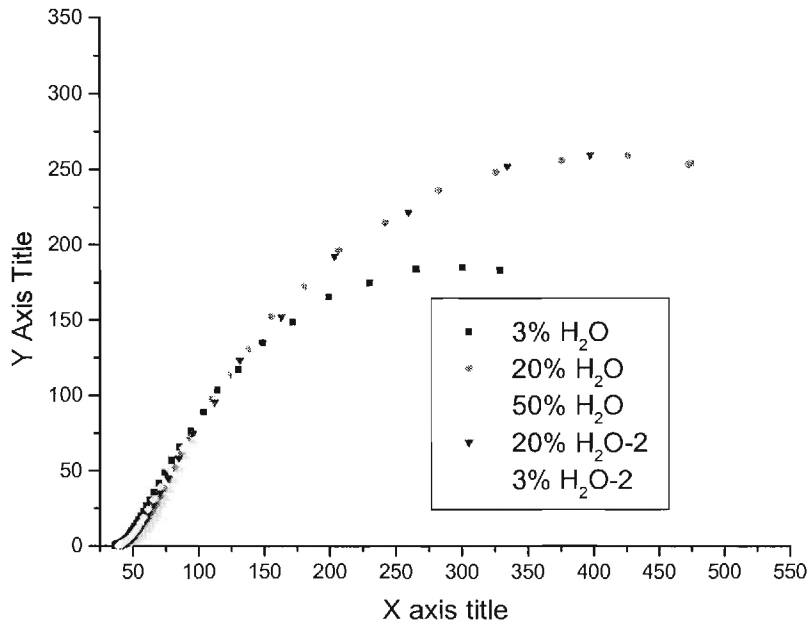

Figure 2.6 *Impedance spectra measured at 500 °C using a two-electrode configuration in humid H_2/Ar atmosphere for a BZCY7 symmetric cell.*

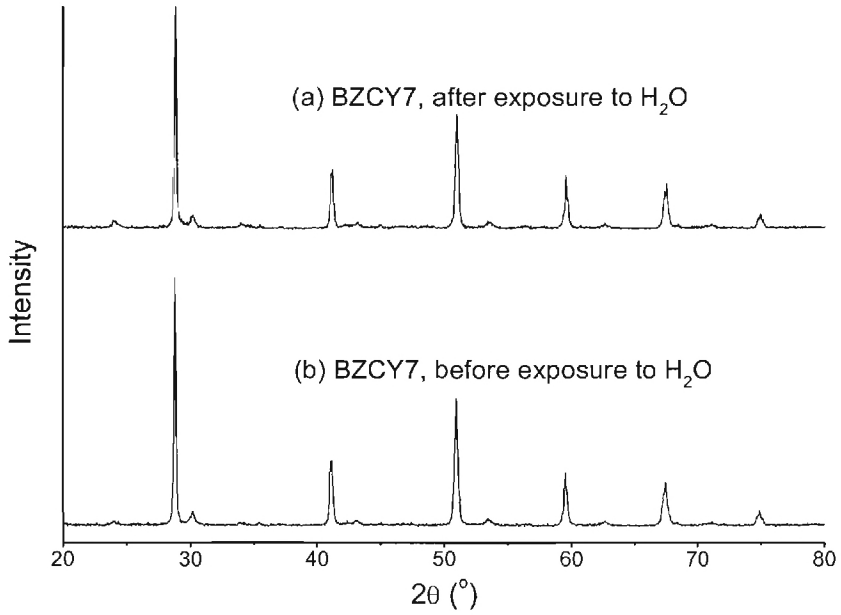

Figure 2.7 *X-ray diffraction patterns for BZCY7 before and after exposure to 50 vol.% H_2O balanced with H_2 at 500 °C.*

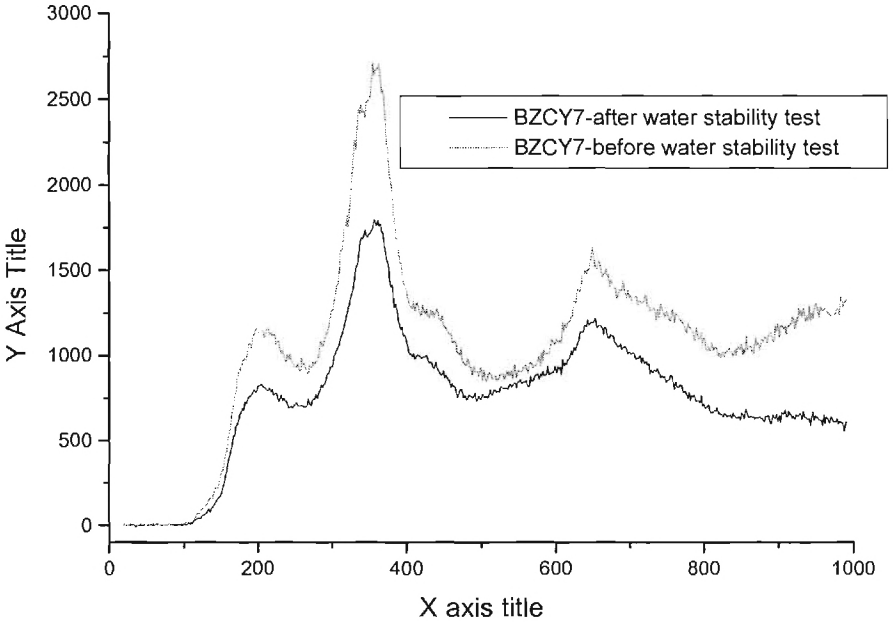

Figure 2.8 *Roman diffraction patterns for BZCY7 before and after exposure to 50 vol.% H_2O balanced with H_2 at 500 °C.*

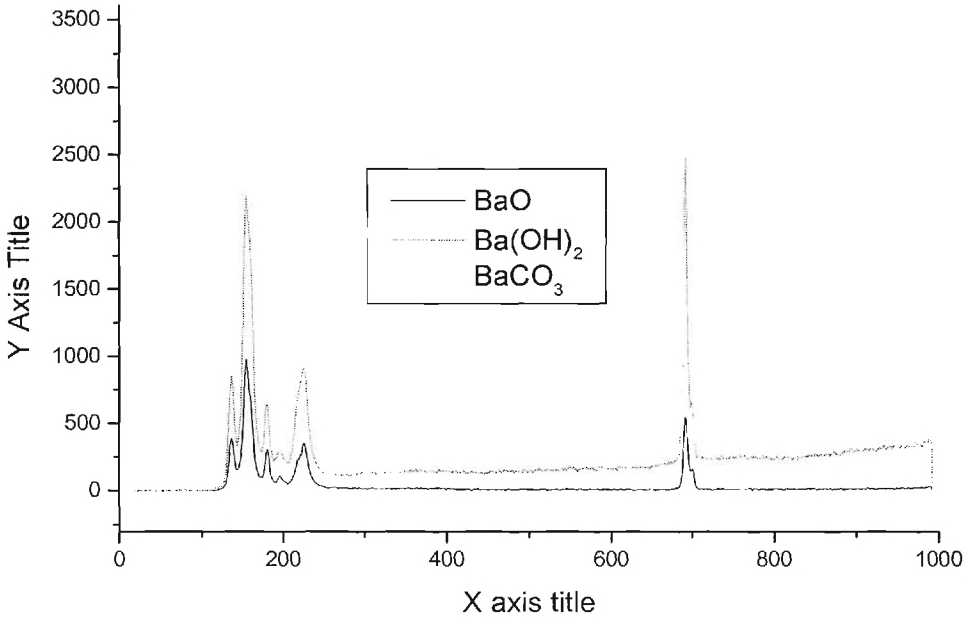

Figure 2.9 *Roman diffraction patterns for BaO, $Ba(OH)_2$, and $BaCO_3$.*

To further confirm there no $Ba(OH)_2$ or BaO formed for BZCY7 after exposed to 50% water vapor containing atmosphere at 500 °C, the Roman examination on BaO, $BaCO_3$, and $Ba(OH)_2$ disk samples were also carried out which was showed in Fig. 2.9. The BaO was made by firing $BaCO_3$ at high temperature, and the $Ba(OH)_2$ was made by boiling BaO in the water. But from the Roman diffraction patterns, it looks like both BaO and $Ba(OH)_2$ are not stable even in the room temperature, and formed $BaCO_3$ with reaction with the CO_2 and H_2O in the air.

2.1.3. Optimization of BZCY7-Ni anode material

The thin electrolyte membrane of BZCY7 on a porous anode of BZCY7-NiO is pressed by means of punches in a hardened metal die. The dry-pressing process is commonly used for pressing parts thicker than 0.5 mm using ordinary powders. To make a 0.5-mm-thick BZCY7 pellet with the commercially available powder, the average thickness of the loose powder in a die is about 1.1 mm. To make a 100-μm-thick BZCY7 film using the same powder, however, the loose powder must be uniformly distributed to form a 220-μm-thick layer during dry pressing, which is very difficult to accomplish. With the foam powder prepared by GNP method, the thickness of the loose powder for making a 10-μm-thick film is 1 mm, which is almost same as that for making a 0.5-mm-thick BZCY7 film with the commercial powder. Thus, it is possible to make thin membranes by dry pressing with foam-structured BZCY7 powder.

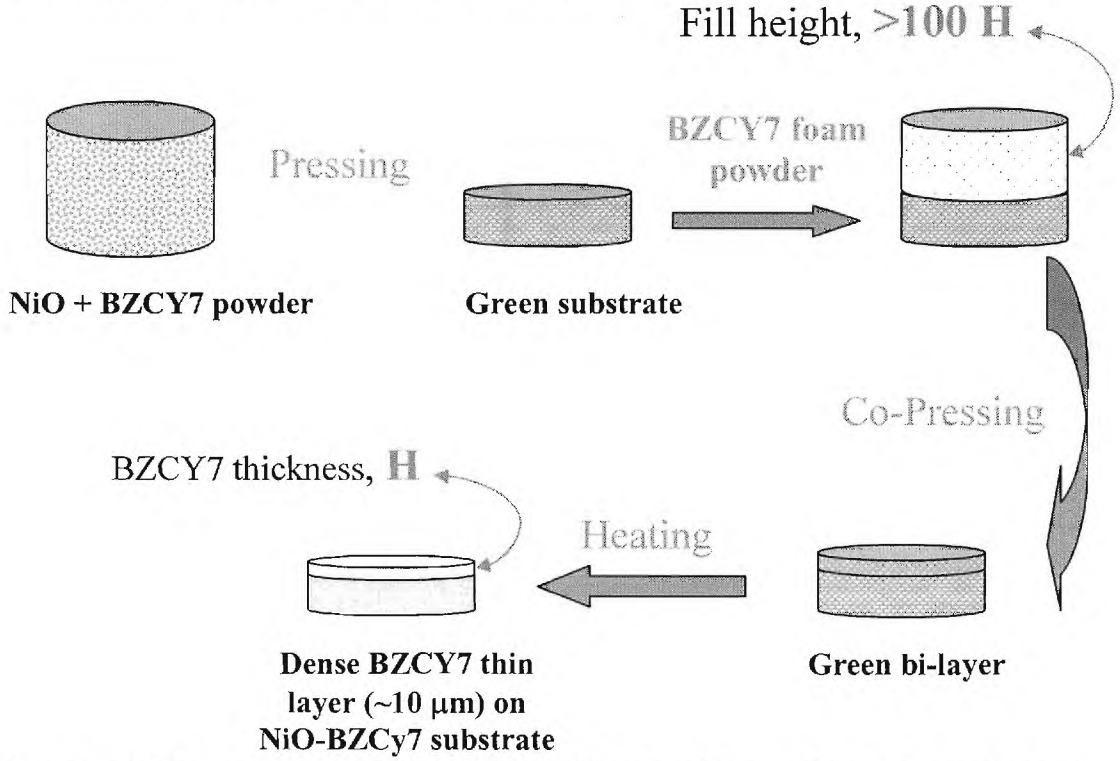

Figure 2.10 *How to make a 10-μm-thick BZCY7 film fabricated by dry pressing with foam-structured BZCY7 powder.*

Figure 2.10 shows a detailed procedure that how to make a 10-μm-thick BZCY7 film fabricated by dry pressing with foam-structured BZCY7 powder. To make a membrane of BZCY7, first, a mixed powder of BZCY7 and NiO (65 wt%) was prepressed at 200 MPa as a substrate, then, highly porous or "foam" BZCY7 powder, synthesized by a glycine nitrate process, was added, distributed uniformly, and uniaxially pressed onto a green substrate of BZCY7-NiO. The bilayer was subsequently sintered at 1350 °C for 5 h, resulting in a BZCY7 membrane on BZCY7/NiO substrate. The thickness of the BZCY7 membrane is controlled by the amount of BZCY7 powder.

Figure 2.11 shows the cross-sectional (Figure 2.9 (a), (b), and (c)) and electrolyte's surface view (Figure 2.9 (d)) of a 20-μm-thick BZCY7 film fabricated by dry pressing with foam-structured BZCY7 powder. The result is kind of out of our expectation, the electrolyte film appear partially porous even after the sintering temperature increased to 1400 °C.

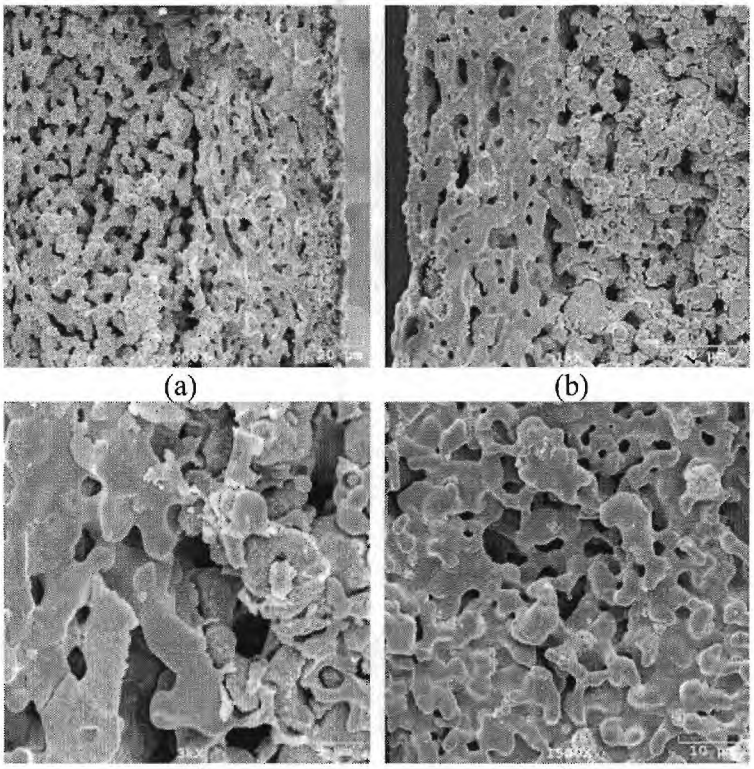

Figure 2.11 *SEM pictures of (a), (b), and (c) a cross-section of a 20-μm-thick BZCY7 film supported on a NiO- BZCY7 substrate, (d) a surface view of partially porous BZCY7 electrolyte.*

According to the references, the powders prepared by glycine-nitrate method should be easy to densify, and GDC and YSZ electrolyte membranes as thin as 8 μm have been prepared and tested in SOFCs by using highly porous or "foam" GDC and YSZ powder which synthesized by a GNP process.

The reason why the sintered electrolyte film is not fully dense is because, that in a dry-pressing process, good powder flow is also essential to uniform volumetric filling and rapid pressing. Dense, nearly spherical particles with smooth surfaces which made by SSR method usually have good flow behavior. However, the BZCY7 powder has very poor flow behavior because it is highly porous and is much finer than 25 μm. Poor flow behavior results inevitably in nonuniform distribution of powder and low packing density, leading to lower density for thinner films. The porosity of the membranes make us failed to further test the fuel cell because the gas leaking through the cross-membrane pinholes.

For the fuel cell performance we reported before, we always use the commercial NiO powder (about 10 μm size) mixed with BZCY7 powder as anode. From the SEM pictures shown in Figure 3.1, we can see that after sintered at 1350 °C, in the anode, the nickel particle size(about 10 μm) is much bigger than the BZCY7 particle size (about 2 μm), the nickel particle and BZCY7 particles are not mixed uniformly, and the porosity of the anode is relatively low.

It is well known that, the microstructure of the electrodes has a critical influence on the performance of the fuel cell. The performance can be improved by optimizing the connectivity and size distribution between particles of each solid phase to yield a larger three-phase (electrode–electrolyte–gas) contract area that is accessible for gas atmospheres.

In order to improve the microstructure of the anode, we started to use fine NiO particles which made by GNP method. The powders of BZCY7 and NiO (made by GNP method) at a weight ratio of 1: 1.92 (volume ratio of 50: 50) were weighted; add 10 and 15 wt% Starch as pore former, respectively, add 2 drops of 5%PVA-H_2O, mixed until the powder is dispersed and looks like sand, then grinded for 1 hour to form an anode precursor. The precursor was pressed in a stainless module to form anode substrate with flat surface, and to possess certain mechanical strength, and then fired at 1350 °C for 6 h.

Figure 2.12 showed that before reduction in the fuel cell testing conditions, the cross-sectional of a BZCY7-Ni anode using NiO powder made by GNP method with 10 and 15 wt% starch as pore former, respectively. We can see the anode with 15% starch mixed as pore former has a slightly higher porosity.

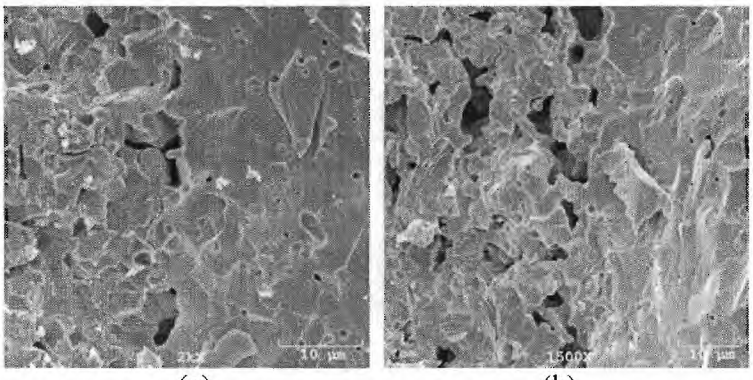

(a) (b)

Figure 2.12 *SEM pictures of the cross-section view of a Ni- BZCY7 (GNP) anode with (a) 10% starch mixed and (b) 15% starch mixed.*

So before reduction, 15% starch-anode has higher porosity than 10% starch-anode. But after reduction of anode, from Fig. 2.13, we can see the porosity of the 15% starch-anode is too high and a crack formed at the interface of electrolyte and anode. So 10% starch-anode is a better choice.

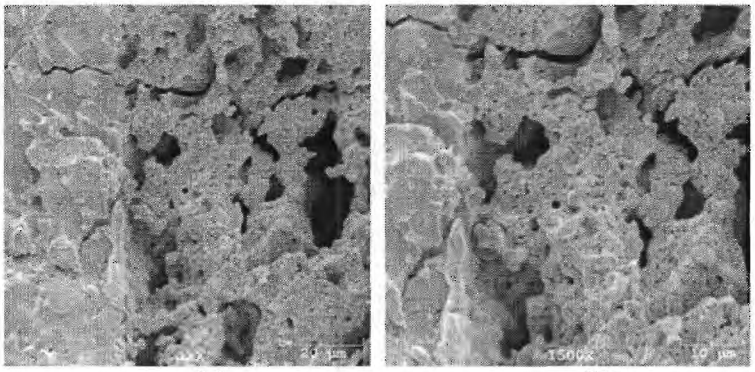

(a) (b)

Figure 2.13 *SEM pictures of the cross-section view of a Ni- BZCY7 (GNP) anode with 15% starch mixed.*

Figure 2.14 shows that after reduction in the fuel cell testing conditions, the cross-sectional SEM pictures (Figure (a) low definition, and (b) high definition) of Ni-BZCY7 anode which made by GNP nickel oxide powders. The anode made by GNP nickel oxide powders has more porosity, higher connectivity, better size distribution between particles of each solid phase, so can yield a larger three-phase (electrode–electrolyte–gas) contract area that is accessible for gas atmospheres.

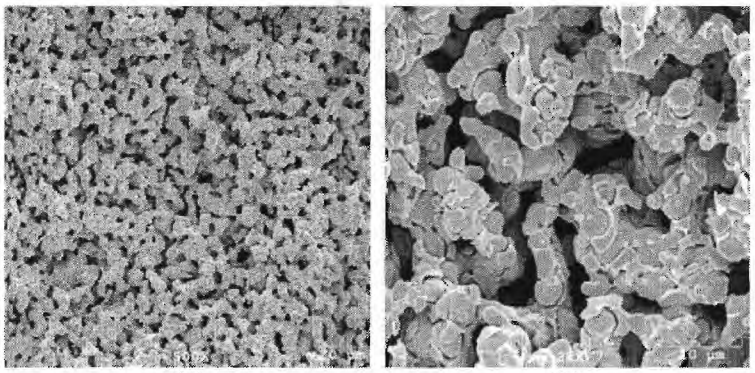

(a) (b)

Figure 2.14 *The cross-sectional SEM pictures (Figure (a) low definition, and (b) high definition) of Ni-BZCY7 anode which made by GNP nickel powders with 12% starch mixed.*

2.1.4. Development of BCPY4 and SSC as Cathode Materials

BCPY4 cathode material: The preliminary results indicate that BCPY4 appear to have the better potential than silver alone as a cathode material for BZCY7 electrolyte based fuel cells. But the impedance analysis indicated that, even use BCPY4 as cathode, the

current limitation for lower operation temperature SOFC based on BZCY7 electrolyte still is high resistance from electrodes, which leads to the relatively poorer fuel cell performance.

Figure 2.15 shows the cross-sectional SEM pictures of each cell component. Some isolated defects such as small voids were observed under SEM investigation. However, no cross-membrane cracks or pinholes were observed. The cathode layer, consisting of sub-micro grains, has an average thickness of 20 μm and a porous porosity of about 40%. The thickness of the porous anode is about 0.5 mm whereas the porosity of the anode was about 30% after the NiO was reduced to Ni.

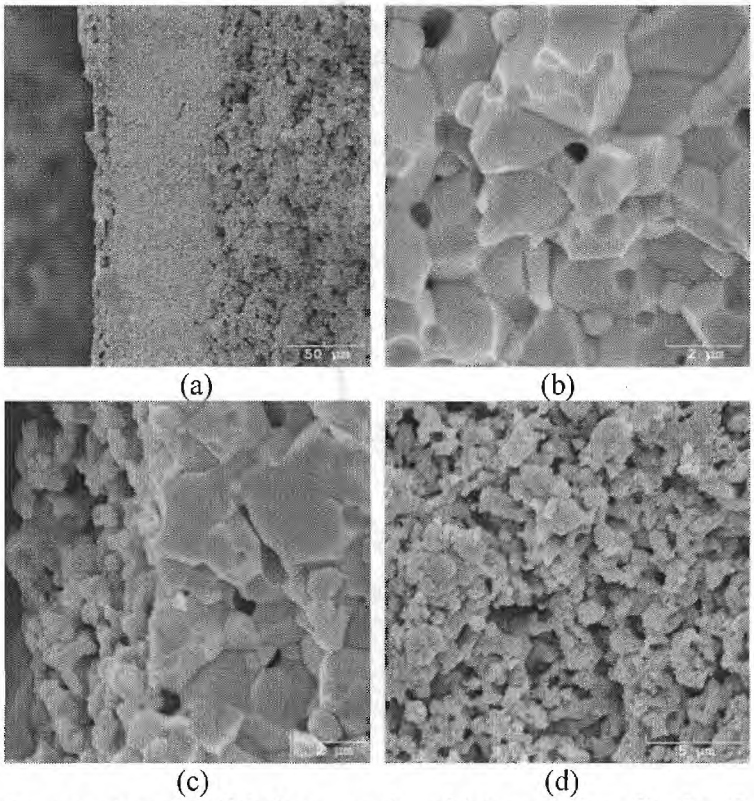

Figure 2.15 *Cross-sectional SEM photographs of (a) a single cell after fuel cell testing, (b) the dense BZCY7 electrolyte, (c) a single cell in cathode BCPY4 side, and surface SEM photograph of (d) porous BCPY4 cathode.*

Shown in Figure 2.16 are three typical impedance spectra measured under open circuit condition at 600, 550, and 500 °C using two-electrode configuration. The intercept with the real axis at high frequencies represents the resistance of the electrolyte and lead wires, whereas the difference between the high-frequency and low-frequency intercepts with the real axis represents the sums of the electrode polarization resistances of the cell. The interfacial resistance includes the contact resistance between the electrode and the electrolyte as well as the resistance to the electrochemical process such as charge transfer and mass transfer. It is about 3.6 Ωcm^2 at 500 °C, which is 2 times higher than the electrolyte resistance. By comparing with the polarization resistances between the SSC-GDC or SSC-SDC cathodes and the GDC electrolyte at 500 °C, which are about 1 Ωcm^2,

clearly, to develop cathode materials with high electro-catalytic activity is a main challenge for the fuel cell based on BZCY7 electrolyte.

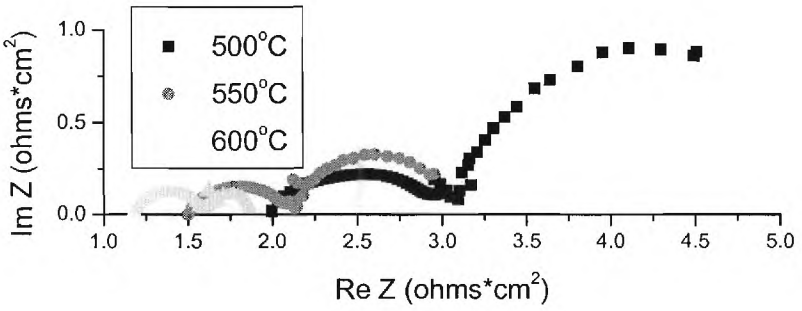

Figure 2.16 *Impedance spectra of a single cell measured under open circuit condition at different temperatures.*

Shown in Figure 2.17 are the interfacial polarization resistances, electrolyte resistances, and total resistances of the cell as determined from the impedance spectra. It is immediately clear that the performance of the cell is influenced by the interfacial resistances, especially at temperatures below 550 °C, where the cell performance is essentially determined by the interfacial resistances. Also, it is clearly seen from Table 2.1 that the ratio of interfacial resistance to total resistance increased dramatically as the operating temperature was reduced, implying that the performance of the SOFCs to be operated at low temperatures depends critically on the interfacial resistance. Accordingly, the development of catalytically active electrodes and interfaces is critical to successful development of SOFCs to be operated at low temperatures (below 550 °C). Mesoporous mixed-conducting electrodes and nanostructured interfaces may significantly improve the performance of low-temperature SOFCs.

	RI/RE	RI/RT
700 °C	39%	28%
650 °C	47%	32%
600 °C	64%	39%
550 °C	108%	52%
500 °C	178%	64%
450 °C	400%	80%

Table 2.1 *The ratio of interfacial resistance to the electrolyte resistance and of interfacial resistance to the total resistance for a cell based on a 65 μm BZCY7 membrane with BCPY4 as cathode.*

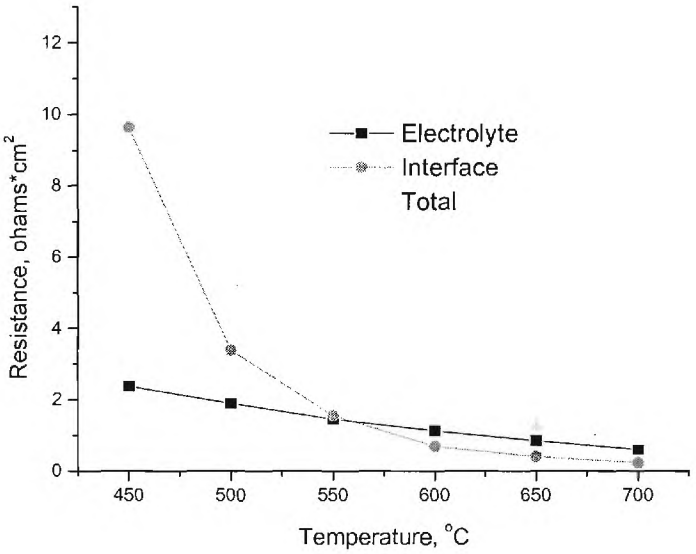

Figure 2.17 *The electrolyte resistances, the interfacial polarization resistance and the total resistance as determined from the impedance spectra for a cell based on a 65 μm BZCY7 membrane with BCPY4 as cathode.*

SSC cathode material: The fuel cell with new cathodes was prepared via a three-step process including anode-electrolyte substrate formation, frame coating, and SSC impregnation.

Firstly, green bi-layer NiO-BZCY7(GNP)/BZCY7(SSC) substrates were prepared by die-pressing at 300 MPa. SSC was made by GNP method and it has extremely low fill density and very fine particle size as shown in Fig. 2.18

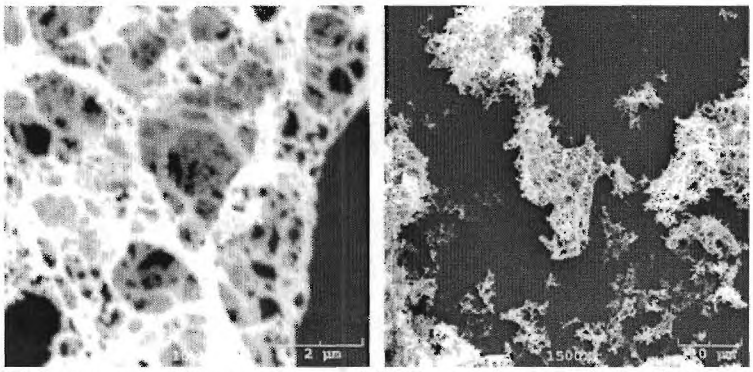

Figure 2.18 *SEM pictures of as-synthesized SSC powders made by GNP method.*

Secondly, the cathode frame was screen-printed onto the green substrate with GNP BZCY7 mixed with 50 wt% starch powder. The powder was grounded with an organic binder in acetone to form uniform BZCY7 slurry. The slurry was subsequently applied to the green substrates with a screen-printing technique. The printed layers were

dried and co-fired with the substrates at 1400 °C for 5 h to form the porous BZCY7 frame on top of a dense substrate as shown in Fig. 2.19.

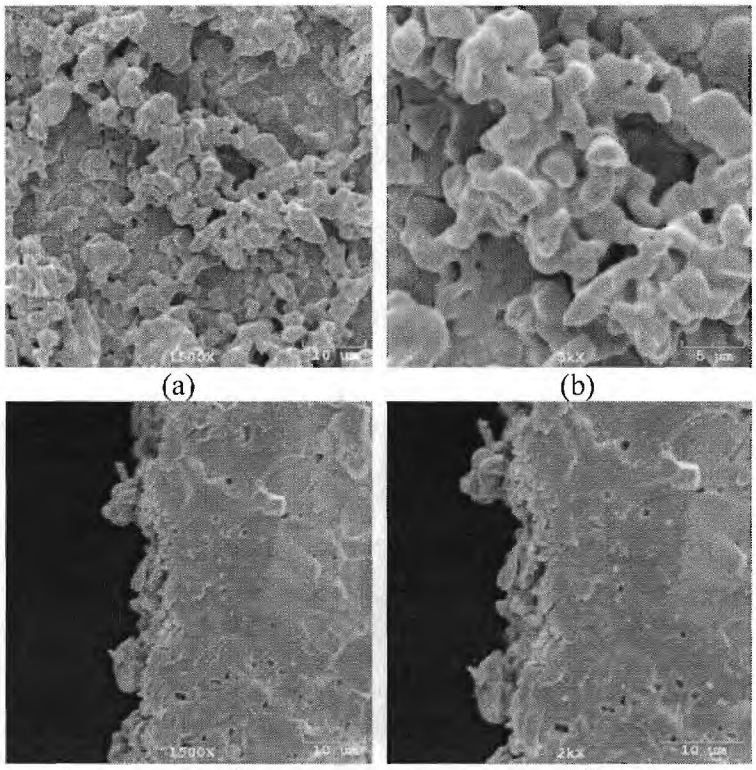

(a) (b)

(c) (d)

Figure 2.19 *Surface SEM pictures ((a) low definition, and (b) high definition), and the cross-sectional SEM pictures ((c) low definition, and (d) high definition) of porous BZCY7 cathode frame layer on top of the dense BZCY electrolyte.*

A layer of SSC was pasted on top of the porous SSC cathode as current collector instead of Ag or Pt as shown in the Fig. 2.20. And the cell was ready for testing in the future.

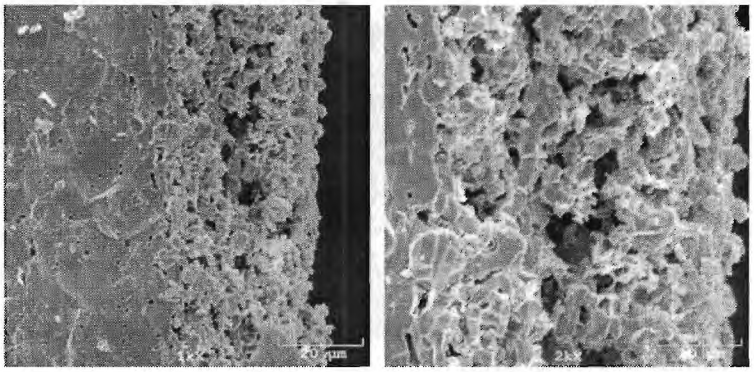

(a) (b)

Figure 2.20 *The cross-sectional SEM pictures ((c) low definition, and (d) high definition) of three layer fuel cell with SSC as the current collector.*

Finally, as shown in Fig. 2.21, SSC was imbedded to the frame with an ion impregnation technique, which was carried out by placing drops of a $SSC(NO_3)x$ nitrate solution (Glycine was added to the solution with a molar ratio of glycine to nitrate at 0.5) on top of the frame. The dropped solution infiltrated to the porous BZCY7 frame by capillary action when it was dripped at room temperature. To introduce sufficient amount of SSC, it was necessary to use multiple impregnations. The impregnated salts were finally heated to 800 °C for 2 h to remove the nitrate ions and organics, and also to form a perovskite SSC.

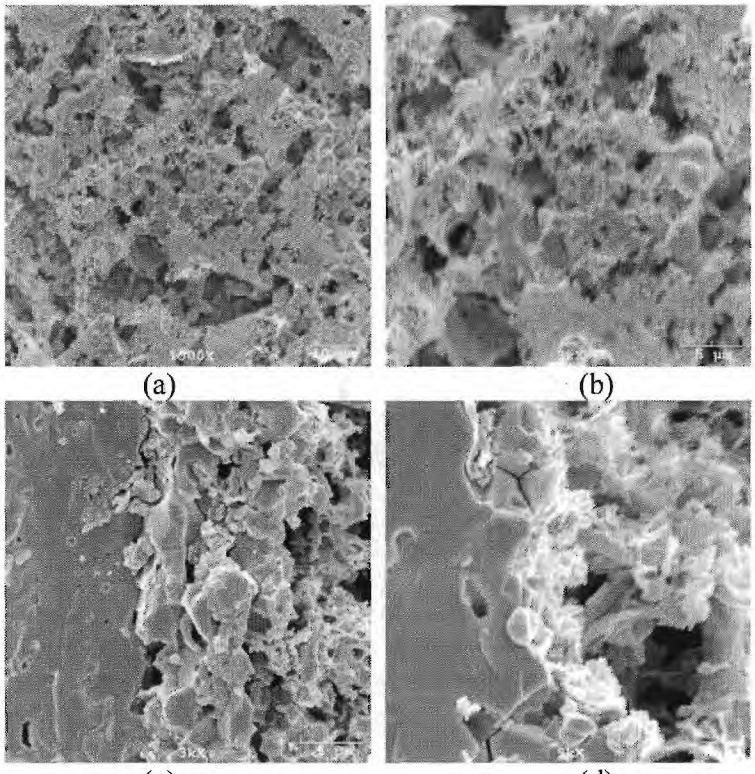

Figure 2.21 *Surface SEM pictures ((a) low definition, and (b) high definition), and the cross-sectional SEM pictures ((c) low definition, and (d) high definition) of porous SSC cathode was imbedded to the cathode frame layer on top of the dense BZCY electrolyte.*

2.1.4 Development of Fuel Cells Based on BZCY7

We fabricated single fuel cells based on BZCY7 electrolyte by modified dry pressing method, which allowed us to obtain a crack-free film with 65 μm thickness even using commercial micro-size BZCY7 powders. Previous fuel cell testing indicated that the cathode-electrolyte interfacial resistance was the determined factor that limited the whole performance. Thus, we further developed a new cathode materials - $Ba(Ce_{0.4}Pr_{0.4}Y_{0.2})O_3$.

When we use mixed electronic and proton conductor BCPY4 as cathode, we still need a metal current collector because the electronic conductivity of BCPY4 is not high enough. At first, we use Ag as current collector, and shown in Figure 2.22 are the current-

voltage characteristics and corresponding power densities for a fuel cell based on a BZCY7 electrolyte membrane of 65 μm thick at different temperatures. Each datum point was recorded about 2 h after cell reached a steady state. Peak power densities were 270, 148, and 56 mW cm^{-2} at 700, 600, and 500 °C, respectively.

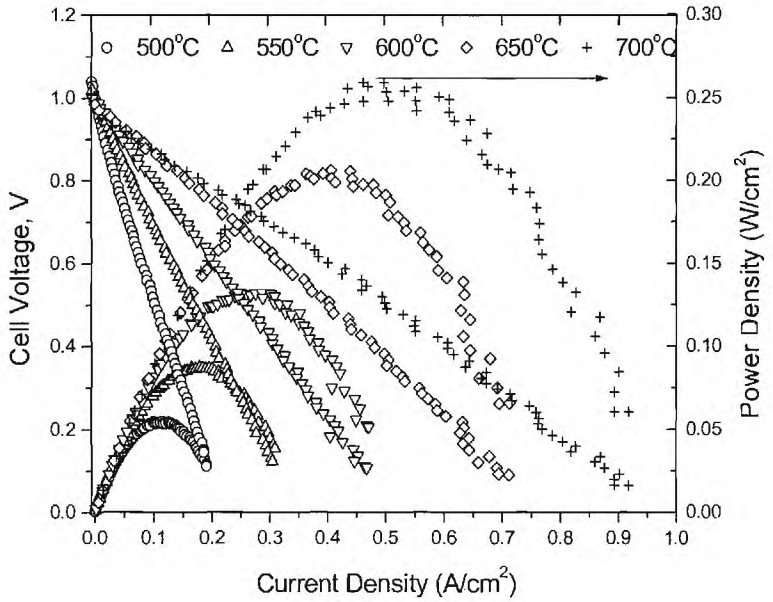

Figure 2.22 *Typical current-voltage characteristics and the corresponding power densities measured at different temperatures for a fuel cell with a BZCY7 electrolyte membrane of 65 μm thick and Ag as current collector.*

After the fuel cell testing, the cell was check by SEM, as shown in Figure 2.23, we found that the silver become dense, which may block the gas-pass-path and then decrease the fuel cell performance.

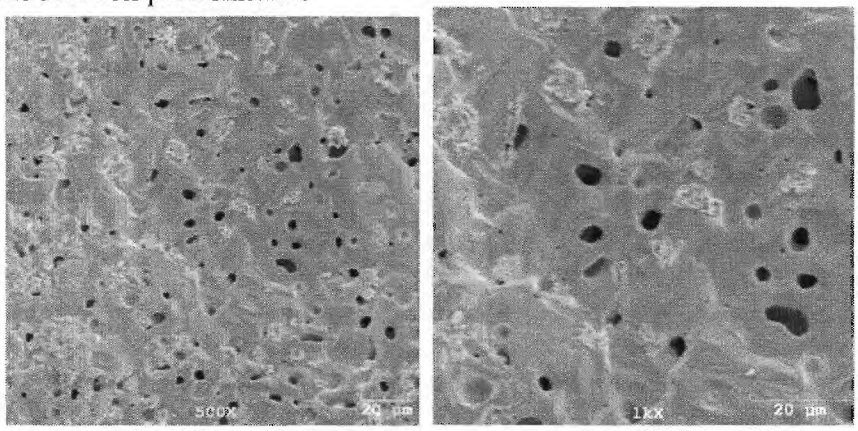

(a) (b)

Figure 2.23 *Surface SEM pictures of an Ag current collector after fuel cell testing.*

We changed to use Pt as current collector, and shown in Figure 2.24 are the corresponding power densities for a fuel cell based on a BZCY7 electrolyte membrane of 85 μm thick at different temperatures. Each datum point was recorded about 2 h after cell reached a steady state. Peak power densities were 246, 156, and 79 mW cm^{-2} at 700, 600, and 500 °C respectively, which is better than the fuel cell performance with Ag as current collector.

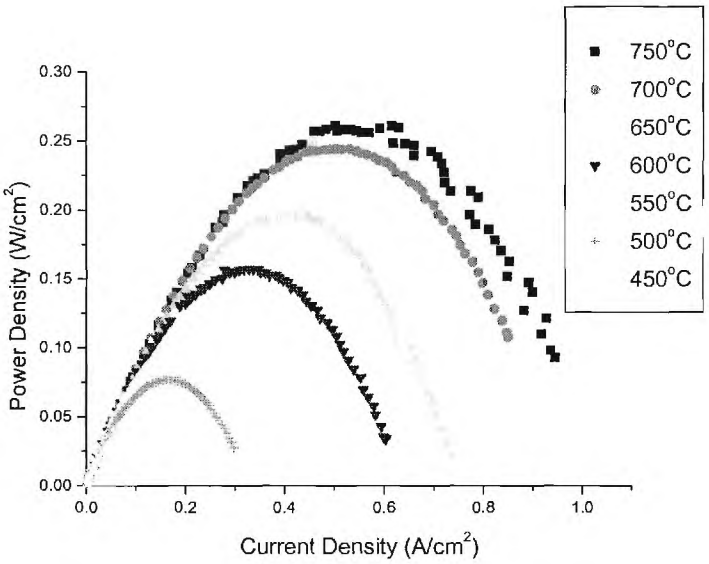

Figure 2.24 *Typical current-voltage characteristics and the corresponding power densities measured at different temperatures for a fuel cell with a BZCY7 electrolyte membrane of 85 μm thick and Pt as current collector.*

After the fuel cell testing, the cell was check by SEM, as shown in Figure 2.25, we found that the Pt still keep partially porous. That might be the reason why we had a better fuel cell performance with Pt as current collector even with a thicker electrolyte film.

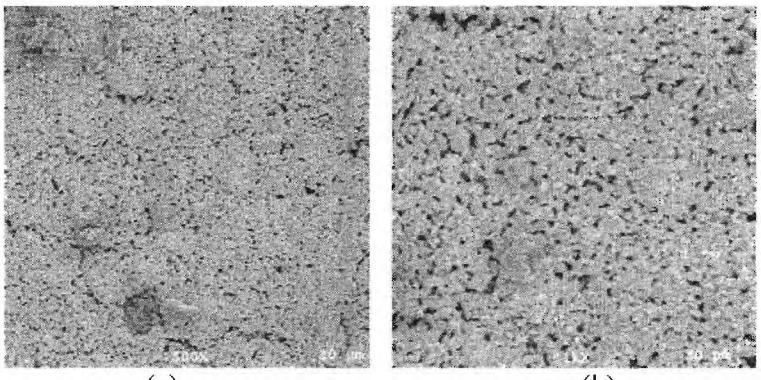

(a) (b)

Figure 2.25 *Surface SEM pictures of a Pt current collector after fuel cell testing.*

A detailed fuel cell performance comparison between using Ag and Pt as current collector was listed as shown in table 2.2. Use Pt instead of Ag as the current collector, the Power density increased about 40% at the low temperature 500 °C. This is because Pt still keeps partially porous at the fuel cell testing condition.

	700°C	600°C	500°C	thickness
Ag as current collector	270 mW cm^{-2}	148 mW cm^{-2}	56 mW cm^{-2}	65 μm
Pt as current collector	246 mW cm^{-2}	156 mW cm^{-2}	79 mW cm^{-2}	85 μm

Table 2.2 *Comparison of the performances of BZCY7 cell with Ag and Pt as current collector.*

2.2. A-site-K-doped (Ba,K)(Zr,Ce,Y)O_3

2.2.1. Optimization of (Ba,K)(Zr,Ce,Y)O_3

An idea of A-site doping by alkali ion instead of the simple A-site optimization in BZCY7 material was proposed. Because the increasing the basicity of the perovskite and thus create more oxygen vacancies, increase the H_2O uptake, and the conductivity. Thus in principle, the alkali oxide (which is very highly basic) should be an effective dopant in the A-site to replace the Ba. In this report, the effect of potassium, as a dopant on the A site of BZCY7 was studied.

Why choose K as a dopant for the Ba in A-site? It is because the similar ionic radius between the Ba^{2+} and K^{1+} (Ba^{2+} -- 1.61, K^{1+}-- 1.64). The similar ionic radius makes it possible to replace the Ba^{2+} with K^{1+} without crushing the perovskite structure of BZCY7 material. And due to the charge difference between Ba^{2+} and K^{1+}, we may create more oxygen vacancies if the K is successfully doped into the A-site of BZCY7.

At first, we tried to use traditional solid state reaction method to fabricate 10% K-doping A-site BZCY7 powders, B9K1ZCY7 [$(Ba_{0.9}K_{0.1})(Ce_{0.7}Zr_{0.1}Y_{0.2})O_3$], but failed. From Fig. 2.26, we clearly can see it is not a single phase material. The reason for that is Potassium carbonate K_2CO_3 has a low melting point 891 °C. So using the conventional solid state procedure may result the loss of potassium due to its easily evaporate at high temperatures.

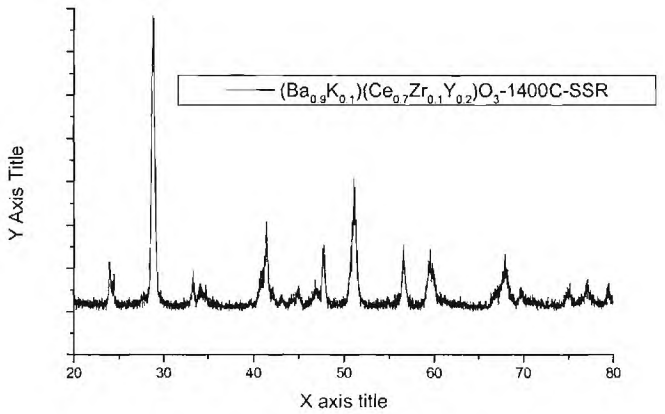

Figure 2.26. *X-ray diffraction patterns of B9K1ZCY7 made by SSR method.*

Since the Solubility in water for potassium nitrate KNO_3 is 35.7 g/100 ml (25 °C), the GNP method was proposed as the reasonable method that might be able to successfully fabricate B9K1ZCY7 single phase material.

The B9K1ZCY7 powder was prepared using a glycine nitrate combustion process. In this process, stoichiometric amounts of KNO_3, $Ba(NO_3)_2$, $Ce(NO_3)_3$, $Y(NO_3)_3$, and $ZrO(NO_3)_2$ were dissolved in water, a suitable HNO_3 (4N) was added to prevent the precipitation of $ZrO(NO_3)_2$. The solution was then mixed with glycine and heated on a hot plate to vaporize water, convert to gel, and finally ignite to flame, resulting in fine ash of pale yellow color. The resultant ash was then fired at 800°C for 2 h to form the "foam" B9K1ZCY7 powder. In here, the NH_2CH_2COOH (glycine) can form complexes with metal ions, prevent selective precipitation, and make the metals mixed at atomic level; it is also the fuel for combustion during the reaction. Below are the reactions:

$$2Ba(NO_3)_2 + 2NH_2CH_2COOH \rightarrow 2BaO + 4CO_2 + 5H_2O + (2N_2 + NO + NO_2)$$

$$2\,KNO_3 + NH_2CH_2COOH \rightarrow K_2O + 4CO_2 + 5H_2O + (2N_2 + NO + NO_2)$$

$$2Ce(NO_3)_3 + 2NH_2CH_2COOH \rightarrow 2CeO_2 + 4CO_2 + 5H_2O + (4N_2 + NO + NO_2)$$

$$2Y(NO_3)_3 + 2NH_2CH_2COOH \rightarrow 2Y_2O_3 + 4CO_2 + 5H_2O + (4N_2 + 2NO + NO_2)$$

$$2ZrO(NO_3)_2 + 2NH_2CH_2COOH \rightarrow 2ZrO_2 + 4CO_2 + 5H_2O + (2N_2 + NO + 2NO_2)$$

The phase purity of the B9K1ZCY7 sample made by GNP methode was also checked by X-ray diffraction measurements. X-ray diffraction results (Figure 2.27 and 2.28) showed that after sintering at 1400 °C in the air and H_2 atmospheres for 6 hours, there are no diffractions indicating an ordering of Ba^{2+} and K^{1+} on the A-site of the ABO_3 perovskite structure, only single perovskite phase diffraction pattern were detected for both sintering processes. This proved that B9K1ZCY7 forms a solid solution with a single perovskite phase like BZCY7, and it is stable in the H_2 atmosphere. This result also confirmed that the Ba^{2+} and K^{1+} in B9K1ZCY7 system are statistically distributed.

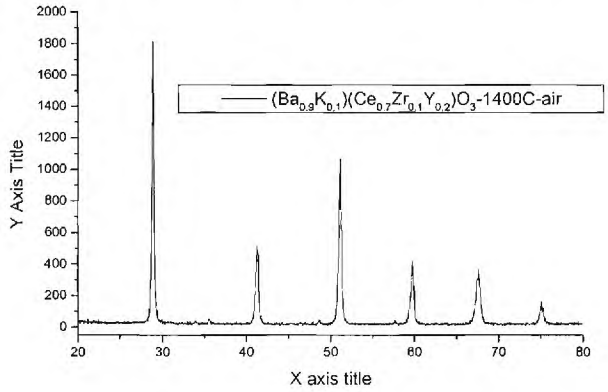

Figure 2.27. *X-ray diffraction patterns of B9K1ZCY7 made by GNP method and sintered at 1400°C in the air atmosphere.*

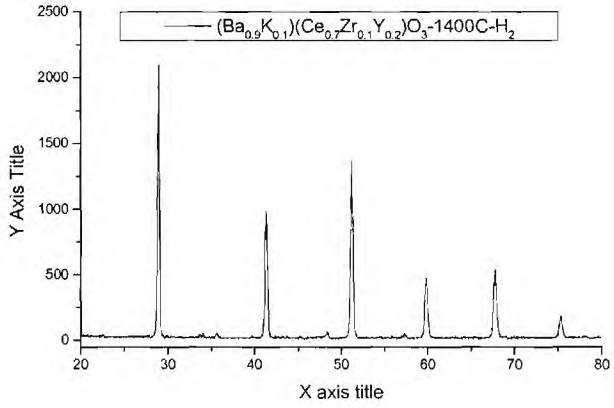

Figure 2.28. *X-ray diffraction patterns of B9K1ZCY7 made by GNP method and sintered at 1400°C in the H_2 atmosphere.*

2.2.2. Conductivity of (Ba,K)(Zr,Ce,Y)O_3

For conductivity measurements, both sides of the sintered disks were polished using 600-grit SiC paper to obtain the desired thickness and produce faces that were flat and parallel to one another. Porous Pt was applied as electrode to both sides of the disc and hardened by firing at 1000 °C for 2 hour. The pellet was then attached to the silver leads of a conductivity cell, which was placed in a tube furnace whose temperature was controlled and measured between 300 and 700 °C. Conductivity was measured in the form of a.c. impedance using a Solartron 1255 HF frequency response analyzer linked to a 1286 electrochemical interface. Typical frequency range was from 0.01 Hz to 1 MHz. The measurement was conducted in a cooling sequence. The prime objectives were to determine the conductivity as a function of temperature.

The conductivity was measured in wet air, humid 4% H_2 balanced Ar, and fuel cell condition, respectively. Water vapor was obtained by bubbling selected gas through deionized water at room temperature (22-23 °C).

As shown in Figure 2.29 are total ionic conductivities of B9K1ZCY7 in various atmospheres (fuel cell condition, wet air and humid 4% H_2 balanced Ar). All the conductivities increased as temperature increased from 300 °C to 700 °C. The conductivity of B9K1ZCY7 in the air atmosphere is relatively high in the high temperatures, but has a much smaller conductivity in the low temperatures due to its high activation enthalpies. This implied that it is an oxygen ion conductor in the air atmosphere. On the other hand, the conductivity of B9K1ZCY7 in the H_2 atmosphere is relatively high in the low temperatures. This implied that it is a proton conductor in the H_2 atmosphere because the transport of proton is much easier than that of oxygen/oxygen vacancy. In this case, protons are not part of the nominal structure or stoichiometry, but are present as foreign species (defects) remaining from synthesis or in equilibrium with ambient hydrogen or water vapor. B9K1ZCY7 has the highest conductivity in fuel cell condition (one side of the disk sample is wet H_2 atmosphere and the other side of the sample is air atmosphere) in the whole temperature range. This implied that it is a mixed

proton-oxygen ion conductor in fuel cell condition and both proton and oxygen ion conductivity have the contribution to the total conductivity.

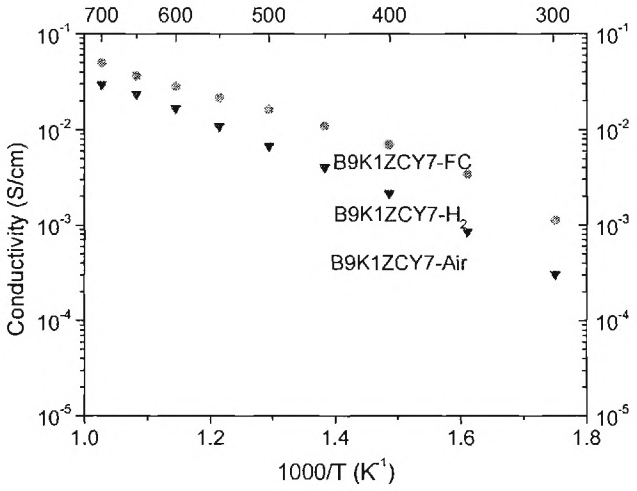

Figure 2.29 *Total ionic conductivity as a function of temperature for B9K1ZCY7 in various atmospheres (fuel cell condition, wet air and humid 4% H_2 balanced Ar).*

By comparing with the conductivity of BZCY7 in humid 4% H_2 balanced Ar atmosphere. As shown in Fig. 2.30, the total ionic conductivities of B9K1ZCY7 is higher than BZCY7 in the whole temperature range (from 300 °C to 700 °C), especially in the high temperatures.

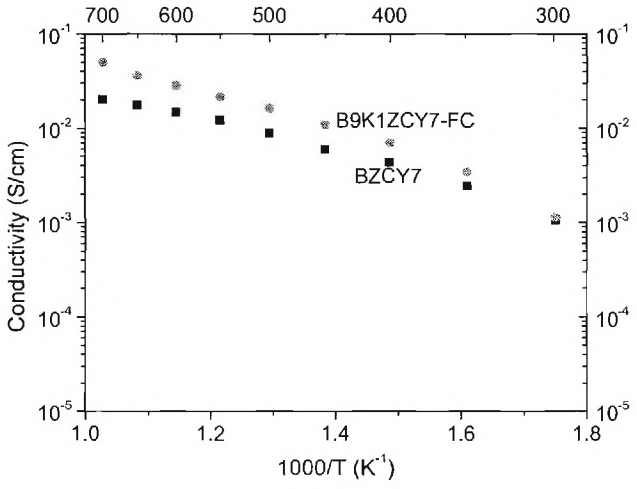

Figure 2.30 *Comparison of the ionic conductivity as a function of temperature for B9K1ZCY7 and BZCY7 electrolyte materials*

The B9K1ZCY7 exhibited the highest ionic conductivities among all known electrolytes viable for solid oxide fuel cell applications. An example of this is the

B9K1ZCY7 has a conductivity of 1.6×10^{-2} S/cm in fuel cell condition at 500 °C, which is about 40 times higher than YSZ and about three times higher than that for LSGM (5×10^{-3} S/cm) and GDC (5×10^{-3} S/cm), as shown in Fig. 2.31

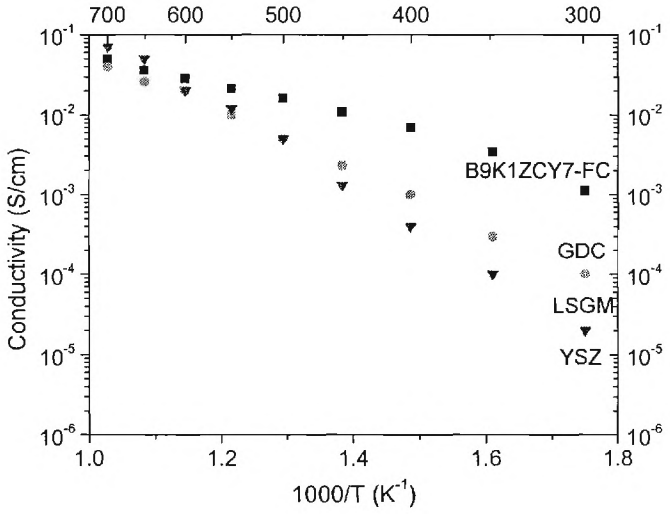

Figure 2.31 *Comparison of the ionic conductivity as a function of temperature for various solid electrolytes.*

By comparing with the conductivity of BZCY7 in humid 4% H_2 balanced Ar atmosphere. As shown in Fig. 2.32, the total conductivities of B9K1ZCY7 in humid 4% H_2 balanced Ar atmosphere is slightly lower than BZCY7 in the lower temperatures, this result implied that the oxygen vacancies produced by A-site doping did not increase the proton conductivity as we expected, but greatly increased the oxygen ion conducvitity.

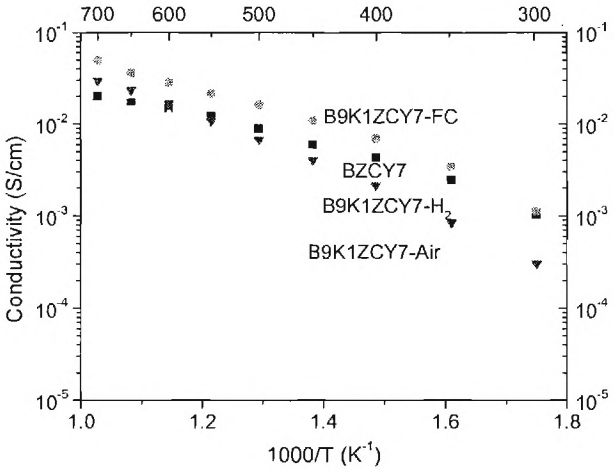

Figure 2.32 *Comparison of the ionic conductivity as a function of temperature for B9K1ZCY7 and BZCY7 electrolyte materials in different atmospheres.*

The attempt of increasing the K-doping content to 20% was tried, B8K2ZCY7 [$(Ba_{0.8}K_{0.2})(Ce_{0.7}Zr_{0.1}Y_{0.2})O_3$], 20% K-doping A-site BZCY7 powders was made by GNP method too. From Fig. 2.33, we can clearly see it is not a single phase material. The second phase ZrO formed. This result showed that the limit of K-doping content is between 10% to 20%.

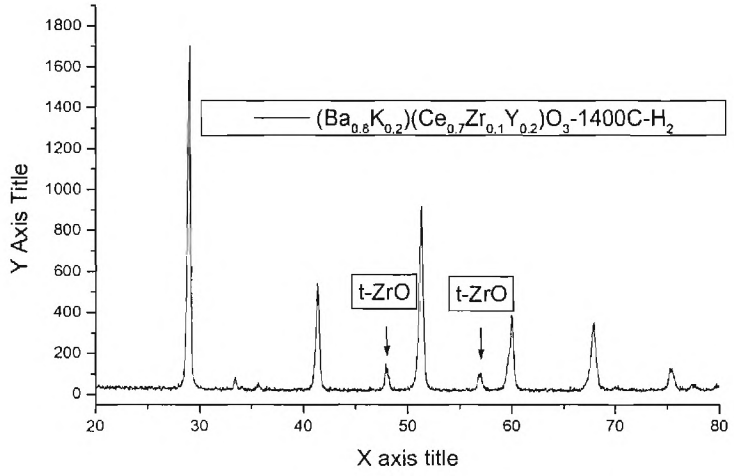

Figure 2.33. *X-ray diffraction pattern of B8K2ZCY7 made by GNP method and sintered at 1400°C in the H_2 atmosphere.*

By comparing with the conductivity of B8K2ZCY7 with B9K1ZCY7 in fuel cell condition, as shown in Fig. 2.34, the total ionic conductivities of B8K2ZCY7 is much lower than B9K1ZCY7 and BZCY7 in the whole temperature range (from 300 °C to 700 °C).

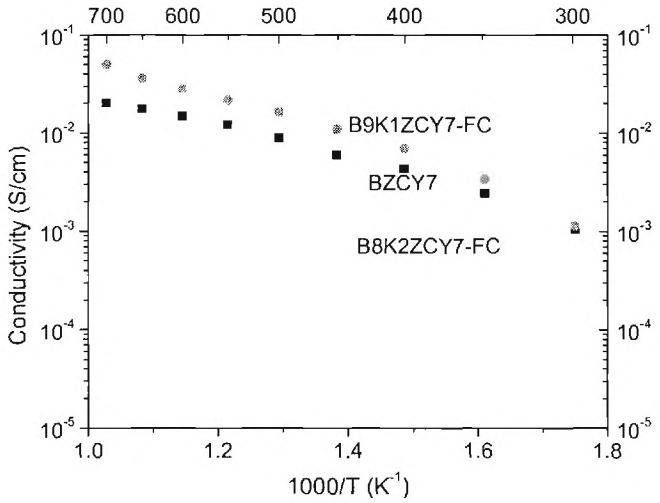

Figure 2.34 *Comparison of the ionic conductivity as a function of temperature for B8K2ZCY7, B9K1ZCY7, and BZCY7 electrolyte materials.*

As shown in Figure 2.35 is total ionic conductivities of B8K2ZCY7 in various atmospheres (fuel cell condition and wet air). All the conductivities increased as temperature increased from 300 °C to 700 °C. The conductivity of B8K2ZCY7 in the fuel cell condition is slightly higher than the conductivity in air atmosphere. This implied that it is an oxygen ion conductor in the fuel cell condition too. Once again, this result implied that the oxygen vacancies produced by A-site doping did not increase the proton conductivity as we expected, but greatly increased the oxygen ion conductivity.

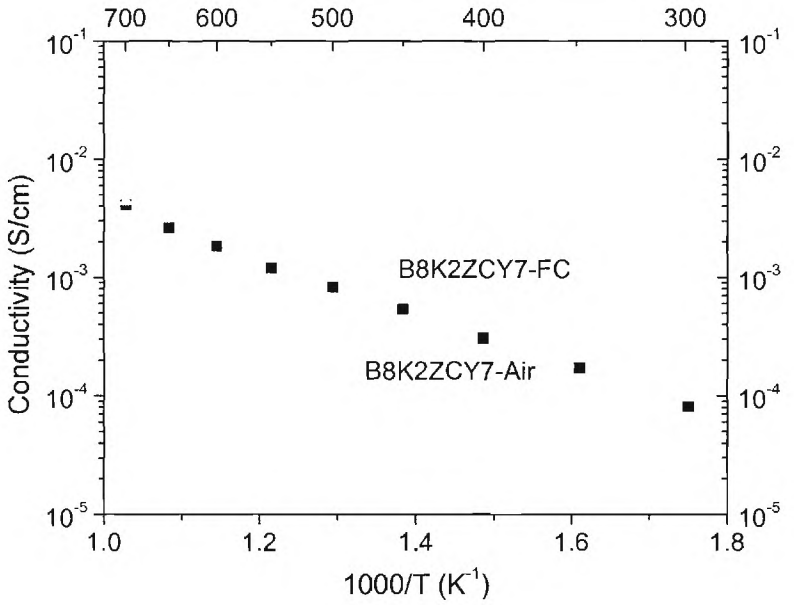

Figure 2.35 *Total ionic conductivity as a function of temperature for B8K2ZCY7 in various atmospheres (fuel cell condition and wet air).*

2.2.3. Development of Fuel Cell Based on BKZCY

Preliminary, 'proof of concept' fuel cell measurements have been conducted using B9K1ZCY7 as the electrolyte. The MEA was comprised of a dense electrolyte with Pt paste deposited on both faces to serve as the electrodes. A single cell with a configuration of Pt | B9K1ZCY7 | Pt with a 1.2 mm thick B9K1ZCY7 electrolyte layer has been demonstrated. The results (see Figure 2.36) show that the gas leaking through the electrolyte film was negligible, and reasonable cell performances were obtained. Maximum power densities are 65, 34, 12 mW cm^{-2}, and the OCV are 1 V, 1.05 V, and 1.04 V at 700, 600, and 500 °C, respectively.